On shotnoise and Brownian motion limits to the accuracy of particle positioning with optical tweezers

Jian Wei Tay[a], Xue Jiang[a] and Warwick P. Bowen[a]

[a]Jack Dodd Centre for Photonics and Ultra-Cold Atoms, Department of Physics, University of Otago, 730, Cumberland St, Dunedin 9016, New Zealand

ABSTRACT

This paper examines the fundamental resolution limit of particle positioning with optical tweezers due to the combined effects of Brownian motion and optical shotnoise. It is found that Brownian motion dominates at low signal frequencies, whilst shotnoise dominates at high frequencies, with the exact crossover frequency varying by many orders of magnitude depending on experimental parameters such as particle size and trapping beam power. These results are significant both for analysis of the bandwidth limits of particle monitoring with optical tweezers and for enhancements of optical tweezer systems based on non-classical states of light.

Keywords: Optical tweezers, split detection, shotnoise, Brownian motion

1. INTRODUCTION

Optical tweezers have many fundamental and commercial applications,[1] ranging from trapping and transportation of cold atoms,[2] to investigations of cellular structure[3] and the properties of DNA.[4] Many of these applications are enabled by their ability to monitor the position of particles with sub-nanometer resolution.[5–7]

Optical tweezers, in their essence, consist of a tightly focused laser beam. In the process of scattering photons a particle in the beam experiences momentum kicks which, if the particle has a refractive index greater than that of the surrounding medium, trap it near the focus of the beam.[8] Interactions of the particle with its surrounding media result in Brownian motion, and consequently uncertainty in the position of the particle. This Brownian motion, as well as motion of the particle due to external forces, can be observed from measurements performed on the forwards and backwards scattered light fields.[6] These measurements are typically implemented with spatially segmented (split) detectors, with uncertainty governed by shotnoise due to the quantisation of the detected field. Hence, the resolution of particle positioning is fundamentally limited both by Brownian motion of the trapped particle and by shotnoise. This paper examines the relative magnitudes of these two noise sources, and the parameter regimes in which each dominates.

Vector diffraction theory[9,10] based numerical calculations are performed to model the optical tweezers trapping and scattered fields in the limit of small particle size. The relative magnitudes of Brownian motion and shotnoise can then be established. We examine the dependence of each noise source on detection frequency, particle radius, particle refractive index, and trapping beam power and focusing. At low signal frequencies Brownian motion dominates for typical experimental parameters. However, the relative contribution from shotnoise increases with detection frequency such that at sufficiently high frequencies shotnoise is always dominant. The crossover frequency between these two regimes was found to vary significantly depending on the exact experimental parameters, ranging from kHz to GHz. This research contributes to the understanding of bandwidth limits of optical tweezers based particle position measurements, and is a first step towards the enhancement of optical tweezers based biological measurements using non-classical states of light.[11,12]

Photonics: Design, Technology, and Packaging III
edited by Wieslaw Z. Krolikowski, Costas M. Soukoulis, Ping Koy Lam, Timothy J. Davis, Shanhui Fan, Yuri S. Kivshar
Proc. of SPIE Vol. 6801, 68010Z, (2008) · 0277-786X/08/$18 · doi: 10.1117/12.769285

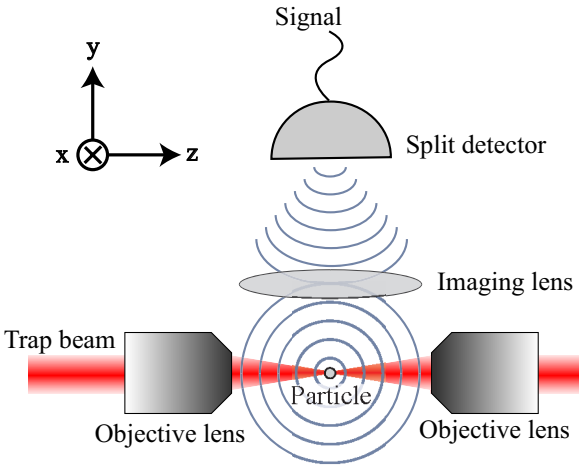

Figure 1. Setup of optical tweezers based particle position measurement. A beam tightly focused by objective lenses forms the optical tweezers and generates a large gradient force trapping a particle at its waist. For a particle smaller than the wavelength, a dipole is induced and light is emitted in the form of radiation. This scattered light is imaged using an appropriate lens onto a split detector, which performs the particle position measurements.

2. METHODOLOGY

2.1 Modelling the system

The two fundamental limits to accuracy of particle positioning with optical tweezers are Brownian motion and shotnoise. Brownian motion is a function of environmental parameters, such as temperature and viscosity of the medium surrounding the trapped particle, and optical trap stiffness, which itself depends on the trapping field in the region of the particle. The shotnoise is a function of the detection configuration and the scattered field and hence also dependent on the trapping field magnitude at the particle position. To fully model the fundamental limits of particle positioning with optical tweezers, we must therefore determine the trapping and scattered fields, as well as the detected signal.

A bright trapping beam is focused by a high numerical aperture (NA) objective lens to form a highly focused waist, defined to be at $\mathbf{r}(x, y, z) = (0, 0, 0)$. A particle in the beam will experience dipole forces which in combination with dissipative forces trap it in the vicinity of the waist. In general, the spatial profile of the scattered field from the particle is complicated but in the limit that the particle size is much less than the wavelength can be approximated by dipole scattering.[13] By monitoring this scattered field, information can be gathered about the position of the particle. In a conventional optical tweezers setup, the particle position is monitored by split detection of the interference between the trapping beam and the scattered field along the axis of the trapping beam (defined as the z-direction in figure 1). We consider a theoretically simpler architecture here and monitor only the off-axis scattering from the particle. As we will show in a later publication, this setup provides significantly enhanced signal-to-noise ratio.[14] Although we do not consider the conventional optical tweezers setup here, our results are directly applicable to that case with only the shotnoise contribution scaling by a constant factor.[14]

2.1.1 Modelling the trapping field

We begin by assuming that the trapping beam is x-polarised (as defined in figure 1), has a TEM_{00} modeshape at 1064 nm and is well-collimated prior to the objective lens. The electric field just prior to the objective lens can then be expressed as

$$\mathbf{E_t}(\mathbf{r_L}) = E_0 \ \exp\left(\frac{-\rho}{w_0^2}\right)\hat{\mathbf{x}} \tag{1}$$

Further author information: (Send correspondence to J.W.T.)
J.W.T.: E-mail: jwtay@physics.otago.ac.nz, Telephone: 64 3 479 7749

where $\mathbf{r_L} = (x, y, z_L)$, z_L is the location of the lens on the z-axis, $\rho = x^2 + y^2$ and w_0 is the waist of the beam. The amplitude E_0 is related to the total power in the trapping beam, P_t, by

$$E_0 = \sqrt{\frac{2P_t}{\pi w_0^2}} \ . \tag{2}$$

Unless otherwise specified, we choose a trapping beam power $P_t = 0.5$ W.

Due to the strongly focused beams required to provide sufficient gradient forces to trap particles in optical tweezers, the paraxial approximation is not valid and scalar diffraction theory cannot accurately predict the trapping field distribution[9] . To model the beam after the objective lens, we use a vector diffraction approach formalised by Richards and Wolf,[10] decomposing the field into a set of plane-waves, each with a unique wave-vector $\mathbf{k}$, amplitude $A(\mathbf{k})$, phase $e^{i\Phi(\mathbf{k})}$ and polarisation $\hat{\mathbf{e_k}}$. In general, the electric field can then be represented by an integral over all space

$$\mathbf{E}(\mathbf{r}) = \int_{-\pi}^{\pi}\int_{0}^{\pi} A(\mathbf{k}) \ \exp^{i[\mathbf{k}\cdot\mathbf{r}+\Phi(\mathbf{k})]} \ \hat{\mathbf{e_k}} \ d\theta \ d\phi \ . \tag{3}$$

Prior to the objective lens, the trapping field is collimated and hence $\Phi_t(\mathbf{k_t}) = 0$. Propagation through the objective lens causes a position dependent phase shift and a rotation of the electric field polarisation. For focusing by an ideal lens, we have after the lens

$$\Phi(\mathbf{k}) = \mathbf{k}\cdot\mathbf{r_L} \ , \tag{4}$$

for the phase and

$$\hat{\mathbf{e_k}} = \frac{(\hat{\mathbf{e_I}}\cdot\hat{\mathbf{n_\perp}})\hat{\mathbf{n_\perp}} + (\hat{\mathbf{e_I}}\cdot\hat{\mathbf{n_\parallel^0}})\hat{\mathbf{n'_\parallel}}}{|(\hat{\mathbf{e_I}}\cdot\hat{\mathbf{n_\perp}})\hat{\mathbf{n_\perp}} + (\hat{\mathbf{e_I}}\cdot\hat{\mathbf{n_\parallel^0}})\hat{\mathbf{n'_\parallel}}|} \ , \tag{5}$$

for the polarisation, where $\hat{\mathbf{e_I}} = \hat{\mathbf{x}}$ is the polarisation of the trapping field prior to the lens and

$$\hat{\mathbf{n_\perp}} = \widehat{\mathbf{k_{out}}\times\mathbf{k_{in}}} \tag{6}$$

$$\hat{\mathbf{n_\parallel^0}} = \widehat{\mathbf{k_{in}}\times\hat{\mathbf{n_\perp}}} \tag{7}$$

$$\hat{\mathbf{n'_\parallel}} = \widehat{\mathbf{k_{out}}\times\hat{\mathbf{n_\perp}}} \tag{8}$$

where $\mathbf{k_{in}}$ is the input wave-vector, $\mathbf{k_{out}}$ is the output wave-vector, $\hat{\mathbf{n_\perp}}$ is the unit vector perpendicular to the plane of incidence, $\hat{\mathbf{n_\parallel^0}}$ the unit vector orthogonal to the plane spanned by $\hat{\mathbf{n_\perp}}$ and $\mathbf{k_{in}}$ and similarly $\hat{\mathbf{n'_\parallel}}$ the unit vector orthogonal to the plane spanned by $\hat{\mathbf{n_\perp}}$ and $\mathbf{k_{out}}$.

It follows that the final form of the electric field integral at the waist of the trapping beam is

$$\mathbf{E_t}(\mathbf{r}) = \int_{-\pi}^{\pi}\int_{0}^{\pi} A_t(\mathbf{k_t}) e^{i[\mathbf{k_t}\cdot\mathbf{r}+\Phi_t(\mathbf{k_t})]} \ d\theta \ d\phi \ \hat{\mathbf{e_t}}(\mathbf{k_t}) \ . \tag{9}$$

The value for $A_t(\mathbf{k_t})$ is found numerically, defined by imposed boundary matching conditions set by the Gaussian input beam. In the model, we set the lenses as having NA = 1 and being perfectly transmissive so no power is lost. It is worth noting here that we have done calculations for NA $\neq$ 1 and arrived at qualitatively identical results.

The integral in Eq. (9) is solved numerically to give the electric field distribution of the trapping beam. Note since the Gaussian beam is an approximate solution to Maxwell's equations, it is not possible to find a solution to them which completely matches the field behaviour after the lens. In general, a boundary condition is chosen to define the field. In our case, we choose the Gaussian field just before the objective lens as the boundary condition. This approach has been shown to be satisfactory.[15]

2.1.2 Modelling the scattered field

Now that the trapping beam has been defined, we can perform the same treatment on the electric field scattered by the particle to obtain the spatial profile of the field arriving at the detector and hence determine both the particle position signal and the shotnoise. As the particle moves away from the beam waist, the scattered field distribution is displaced in the opposite direction. By monitoring this shift in position, the displacement of the particle in the beam is able to be inferred. As mentioned earlier, we consider only particles with radii a much smaller than the optical wavelength ($a \ll \lambda$) and hence model the scattered field by dipole radiation which has an electric field given by[16]

$$\mathbf{E_S}(\mathbf{r}) = \frac{\mathrm{e}^{ik_s r}}{-ik_s r}\frac{ik_s^3}{4\pi\epsilon_m}\hat{\mathbf{e_r}} \times \hat{\mathbf{e_r}} \times \mathbf{p} \ , \tag{10}$$

where the dipole moment of the particle $\mathbf{p}$ is given by

$$\mathbf{p} = 4\pi\epsilon_m a^3 \frac{\epsilon_1 - \epsilon_2}{\epsilon_1 + 2\epsilon_2}\mathbf{E_0} \ , \tag{11}$$

with $\hat{\mathbf{e_r}}(x, y, z)$ the unit vector from the particle to the point $\mathbf{r}(x, y, z)$. ϵ_1 and ϵ_2 are the dielectric constants of the particle and the surrounding environment respectively. The dielectric constant and refractive index of a material are related by $\epsilon = n^2$. For simplicity, we assume the particle motion is confined to the x-axis, with a displacement from the centre of the trap of Δx. Hence the field experienced by the dipole is $\mathbf{E_0} = \mathbf{E_t}(\Delta x, 0, 0)$, obtained from the calculated electric field distribution of the trap field.

We once again apply the vector diffraction formalism and decompose the scattered field into a set of plane waves. Each wave is propagated through an imaging lens to the image plane, giving the integral for the scattered field at the image plane as

$$\mathbf{E_s}(\mathbf{r}) = \int_{-\pi}^{\pi}\int_{0}^{\pi} A_s(\mathbf{k_s})\ \mathrm{e}^{i[\mathbf{k_s}\cdot\mathbf{r} + \Phi_s(\mathbf{k_s})]}\ \hat{\mathbf{e_s}}(\mathbf{k_s})\ d\theta\ d\phi \ , \tag{12}$$

where where $\mathbf{k_s}$ is the wave-vector of the scattered field. As before, the amplitude $A_s(\mathbf{k_s})$ is determined numerically and defined by the boundary matching condition from the intial scattered fields. The phase $\Phi_s(\mathbf{k_s})$ is given by

$$\Phi_s(\mathbf{k_s}) = \mathbf{k_s} \cdot \mathbf{r_I} \ , \tag{13}$$

where $\mathbf{r_I}(x, y, z)$ is the focal point of the imaging lens. The lens is chosen such that the distance from the lens to the particle is twice its focal length (F), giving an image the same distance (2F) away on the other side of the lens. Hence we find that the final polarisation is given by

$$\hat{\mathbf{e_s}}(\mathbf{k_s}) = (\hat{\mathbf{e_I}}(\mathbf{k_I})_x, -\hat{\mathbf{e_I}}(\mathbf{k_I})_y, \hat{\mathbf{e_I}}(\mathbf{k_I})_z) \ , \tag{14}$$

where the initial scattered field polarisation $\hat{\mathbf{e_I}}(\mathbf{k_I})$ is

$$\hat{\mathbf{e_I}}(\mathbf{k_I}) = \widehat{\hat{\mathbf{e_r}} \times \hat{\mathbf{e_r}} \times \mathbf{p}} \tag{15}$$

as defined in Eq. (10). The electric field of the scattered light at the image plane is then solved numerically as before.

We choose the detector position to match the image plane of the imaging lens. The average intensity incident on the detector is then given by

$$P_s = \langle \mathbf{S} \rangle \cdot \hat{\mathbf{y}} \tag{16}$$

$$= \frac{1}{2}\mathrm{Re}\left\{\mathbf{E_s} \times \mathbf{H_s^*}\right\} \cdot \hat{\mathbf{y}} \ . \tag{17}$$

The magnetic field $\mathbf{H_s}$ is easily obtained by decomposing into a set of plane-waves analogous to the electric field, where the magnetic and electric fields of a plane electromagnetic wave are related by

$$\mathbf{H} = \frac{\mathbf{k} \times \mathbf{E}}{\Omega\mu_0} \tag{18}$$

with $\Omega = 2\pi\nu$, the angular frequency of the light. Hence at the image plane, the magnetic field of the scattered light is obtained by numerically solving the integral

$$\mathbf{H_s}(\mathbf{r}) = \int_{-\pi}^{\pi}\int_{0}^{\pi} B_s(\mathbf{k_s})\ \mathrm{e}^{i[\mathbf{k_s}\cdot\mathbf{r}+\Phi_s(\mathbf{k_s})]}\ \hat{\boldsymbol{\epsilon}}_\mathbf{s}(\mathbf{k_s})\ d\theta\ d\phi\ , \tag{19}$$

where $B_s(\mathbf{k_s})$ is the magnetic field amplitude of each plane-wave.

The output signal from each half of the split detector is proportional to the number of incident scattered photons per second

$$N_A = \frac{1}{\hbar\omega}\int_{-\infty}^{\infty} dy \int_{0}^{\infty} dx\ \frac{1}{2}\mathrm{Re}\left(\mathbf{E_s}\times\mathbf{H_s}^*\right)\cdot\hat{\mathbf{y}} \tag{20}$$

$$N_B = \frac{1}{\hbar\omega}\int_{-\infty}^{\infty} dy \int_{-\infty}^{0} dx\ \frac{1}{2}\mathrm{Re}\left(\mathbf{E_s}\times\mathbf{H_s}^*\right)\cdot\hat{\mathbf{y}} \tag{21}$$

where the subscripts A and B label the two halves of the split detector. We have taken the detector to be much larger than the focal spot in the imaged field such that all the light arriving at the image plane is detected. The final output signal is proportional to the photon number difference per second

$$\Delta N = N_A - N_B\ . \tag{22}$$

The total number of photons arriving at the image plane per second is of course

$$N = N_A + N_B\ , \tag{23}$$

and is related to the total power scattered by the dipole, P_s, in the forward direction by

$$N = \frac{P_s}{h\nu}\ . \tag{24}$$

P_s is defined by[17]

$$\mathbf{P_s} = \frac{k^4 a^6 \pi}{\eta}\left(\frac{\epsilon_1-\epsilon_m}{\epsilon_1+2\epsilon_m}\right)^2 |\mathbf{E_t}(\Delta\mathrm{x},0,0)|^2 \tag{25}$$

where $\eta = \sqrt{\mu_0\epsilon_0^{-1}}$.

2.2 Particle positioning uncertainty due to shotnoise

The split detector is initially aligned such that when the particle is at the origin, the signal is zero. Figure 2 shows the photon number difference per second between two halves of a split detector measuring the scattered field as obtained from our numerical calculations. The scattered power is dependent on $|\mathbf{E_t}(\Delta\mathrm{x},0,0)|^2$ which for large particle displacements causes a roll-off in detected signal as can be seen in figure 2. A linear relationship exists between detector signal and particle position for small displacements on either side of the origin. Hence we can define in this region of small displacement

$$\Delta N = \xi\Delta x \tag{26}$$

where ξ is the slope of the signal about the origin. As mentioned earlier, we assume that the particle is only ever displaced along the x-axis, although this is easily generalisable to displacements along both the y- and z- axes.

Rearranging in terms of displacement, we can take the variance of both sides to give

$$\left\langle(\Delta x)^2\right\rangle_S = \xi^{-2}\left\langle(\Delta N)^2\right\rangle \tag{27}$$

For shotnoise limited light, the variance $\left\langle(\Delta N)^2\right\rangle$ is just the total number of photons incident on the detector per second, N, giving the particle positioning variance due to shotnoise as

$$\left\langle(\Delta x)^2\right\rangle_S = \frac{N}{\xi^2} \tag{28}$$

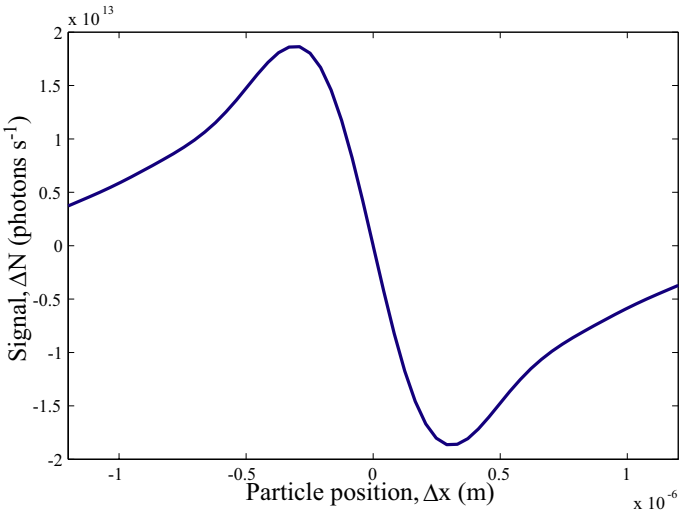

Figure 2. Typical signal measured using a split detector with particle position within the optical tweezers. Here we have used a particle of radius 100 nm with refractive index of 1.4, placed in a 0.5 W trapping beam with a waist of 4 μm.

2.3 Particle positioning uncertainty due to Brownian motion

A particle trapped in optical tweezers is buffeted by thermal motion of the surrounding fluid giving rise to Brownian motion. The Langevin equation describing the system is as for a weak trapping potential[18]

$$\ddot{x}(t) = -\frac{\beta}{m}\dot{x}(t) - \frac{k_s}{m}x(t) + \frac{\sqrt{f}}{m}\gamma(t) \ , \tag{29}$$

where β is the drag coefficient, k_s the trap stiffness, m the mass of the particle and f, the coefficient of the random motion γ, representing the amplitude of the buffeting by thermal motion. The Fourier transform of this equation provides a power spectral density response of the particle position with driving frequency ω

$$-\omega^2 x(\omega) = \sqrt{\frac{f}{m}}\gamma(\omega) - i\omega\frac{\beta}{m}x(\omega) - \frac{k_s}{m}x(\omega) \ , \tag{30}$$

where β, f and m are given by

$$\beta = 6\pi a\eta \tag{31}$$
$$f = 12\pi a\eta k_B T \tag{32}$$
$$m = \rho\left(\frac{4}{3}\pi a^3\right) \tag{33}$$

and η is the viscosity of the medium surrounding the particle, T the temperature, ρ the density of the particle and a the radius of the dipole, which we have assumed spherical. For our calculations we assume the particle is submerged in water giving $\eta = 10^{-3}$ Pa·s, at a temperature of 20°C. The particle is assumed to be fused silica with a density $\rho = 2.2$ g/mol. The spring constant k_s is derived from the gradient force acting on the particle[19]

$$\mathbf{F}(\mathbf{r}) = 2\pi n_2^2 \epsilon_0 a^3 \left(\frac{m^2-1}{m^2+2}\right)\nabla|\mathbf{E_t}^2(\mathbf{r})| \ , \tag{34}$$

where n_2 is the refractive index of surrounding fluid and m is the ratio of refractive indices $\frac{n_1}{n_2}$. The refractive indices unless otherwise specified are $n_1 = 1.456$ for the particle and $n_2 = 1.333$ for the surrounding fluid. The value of $|\mathbf{E_t}^2|$ here is given by the electric field of the trapping beam at the particle position as previously calculated. Thus for displacements in the x-direction

$$k_s = \frac{dF_x}{dx} \ . \tag{35}$$

Rearranging Eq. (30) for x, using $\beta' = \frac{\beta}{m}$, $f' = \frac{f}{m}$, $k'_s = \frac{k_s}{m}$ and neglecting to explicitly denote the frequency dependence we get

$$x = \frac{\sqrt{f'}\,\gamma}{(k'_s - \omega^2) + i\omega\beta'} \ . \tag{36}$$

The variance of the Brownian motion is then

$$\left\langle (\Delta x)^2 \right\rangle_B = \frac{f'}{\left(k'_s - \omega^2\right)^2 + \omega^2\beta'^2} \langle \gamma\gamma^* \rangle \tag{37}$$

$$= \frac{f'}{\left(k'_s - \omega^2\right)^2 + \omega^2\beta'^2} \tag{38}$$

where since Brownian motion is a stochastic process, $\langle \gamma(t)\gamma(t')^* \rangle = \delta(t - t')$.

Assuming that the inertial forces are negligible at low driving frequencies, the critical angular frequency of the particle is given by

$$\omega_C = \frac{k}{\beta} \ . \tag{39}$$

This represents the frequency at which the amplitude of the power spectral density (PSD) response of the particle due to Brownian motion is half the maximum.For low angular frequencies $\omega \ll \omega_C$, the response of the particle is constant while at higher frequencies $\omega \gg \omega_C$, the PSD falls off with ω_C^{-2}. This shows that the particle is not affected by external forces with high frequencies.[20]

3. RESULTS

3.1 Power spectral density

The total power spectral density (PSD) of the particle positioning variance is the sum of contributions due to both shotnoise and Brownian motion

$$\langle (\Delta x)^2 \rangle = \langle (\Delta x)^2 \rangle_S + \langle (\Delta x^2) \rangle_B \ , \tag{40}$$

since the two are independent processes. Figure 3 shows the PSD over a range of angular frequencies for three particle sizes, along with the shotnoise and Brownian motion components. we see that at low detection frequencies Brownian motion is always the dominant noise source. However as the detection frequency increases, the relative magnitude of the contribution from shotnoise increases with shotnoise becoming the dominant noise source at sufficiently high frequencies. The critical frequency for each particle size is given in the caption however note that for (iv), the critical frequency is 13 rad s^{-1} and the variance is approximately constant at frequencies much less than this. The constant regions for cases (ii) and (iii) cannot be seen at the given axis resolution.

3.2 Crossover frequency

To characterise where the contribution to the particle positioning uncertainty from shotnoise dominates over that from Brownian motion, the angular frequency at which the two noise sources have equal magnitude was calculated. This crossover frequency was found for varying experimental parameters including the radius and refractive index of the particle, as well as the power and waist size of the trapping beam and is shown in figure 4. The critical frequency of each configuration is shown on the same plots for comparison.

Above the crossover frequency, shotnoise is the dominant noise source. We find that the crossover frequencies varies dramatically with experimental parameters, with frequencies ranging from kHz to GHz. We found the crossover frequencies increased as dipole size, trapping beam power and particle refractive index were increased. This was expected since the dependence of N and ξ on these parameters results in scaling of the shotnoise with $\frac{1}{a^6}$, $\frac{1}{P_t}$ and $\frac{1}{C_m}$ where

$$C_m = \left(\frac{\epsilon_1 - \epsilon_2}{\epsilon_1 + 2\epsilon_2} \right)^2 \tag{41}$$

is used to denote the contribution due to material constants. In contrast, the crossover and critical frequencies go down as the waist of the trapping beam is increased.

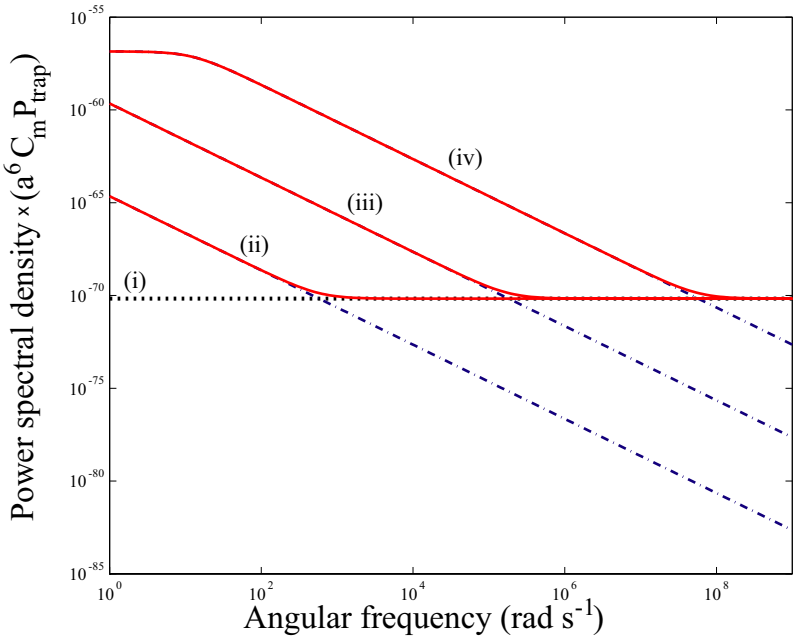

Figure 3. The power spectral density of particle positioning uncertainty due to shotnoise and Brownian motion for (ii) $a = 1$ nm, (iii) $a = 10$ nm and (iv) $a = 100$ nm. The shotnoise is normalised for dipole size, material refractive index and trap beam power in each case to yield a flat line (i) independent of experimental parameters. The same normalisation is applied to the Brownian motion. For each case, the solid line represents the total PSD, while the dot-dashed lines indicate the contribution due to Brownian motion. The critical frequency for each particle size is (ii) 0.0013 rad s^{-1}, (iii) 0.13 rad s^{-1} and (iv) 13rad s^{-1}, respectively.

4. CONCLUSION

We have developed a vector diffraction theory model for optical tweezers based particle positioning. Using this model, we have determined the relative magnitudes of the particle positioning error due to Brownian motion and shotnoise for a range of experimental parameters. At low signal frequencies Brownian motion is found to be the dominant noise source. However, at high frequencies the Brownian motion is surpassed by shotnoise. The crossover frequency between the two regimes is found to vary by many orders of magnitude depending on the exact experimental parameters. Our results contribute to the understanding of fundamental limits to the bandwidth of optical tweezers based particle position measurements, and facilitate progress towards the enhancement of optical tweezers devices using non-classical fields.

5. ACKNOWLEDGEMENTS

This research was supported by the New Zealand Foundation for Research Science and Technology under the contract NERF-UOOX0703: Quantum Technologies, and by the Royal Society of New Zealand Marsden Fund.

REFERENCES

1. For a good review see: D. G. Grier, "A revolution in optical manipulation", Nature, **424**, pp. 810, 2003.
2. I. Dotsenko, W. Alt, M. Khudaverdyan, S. Kuhr, D. Meschede, Y. Miroshnychenko, D. Schrader, and A. Rauschenbeutel, "Submicrometer position control of single trapped neutral atoms", Phys. Rev. Lett., **95**, pp. 033002, 2005.
3. A. I. Bishop, T. A. Nieminen, N. R. Heckenberg, and Halina Rubinsztein-Dunlop, "Optical microrheology using rotating laser-trapped particles", Phys. Rev. Lett., **92**, pp. 198104, 2004.
4. See for example: X. Zhuang, "Unraveling DNA condensation with optical tweezers", Nature, **305**, pp. 188, 2004; C. Bustamante, Z. Bryant, S. B. Smith, "Ten years of tension: single-molecule DNA mechanics", Nature, **421**, pp. 423, 2003.

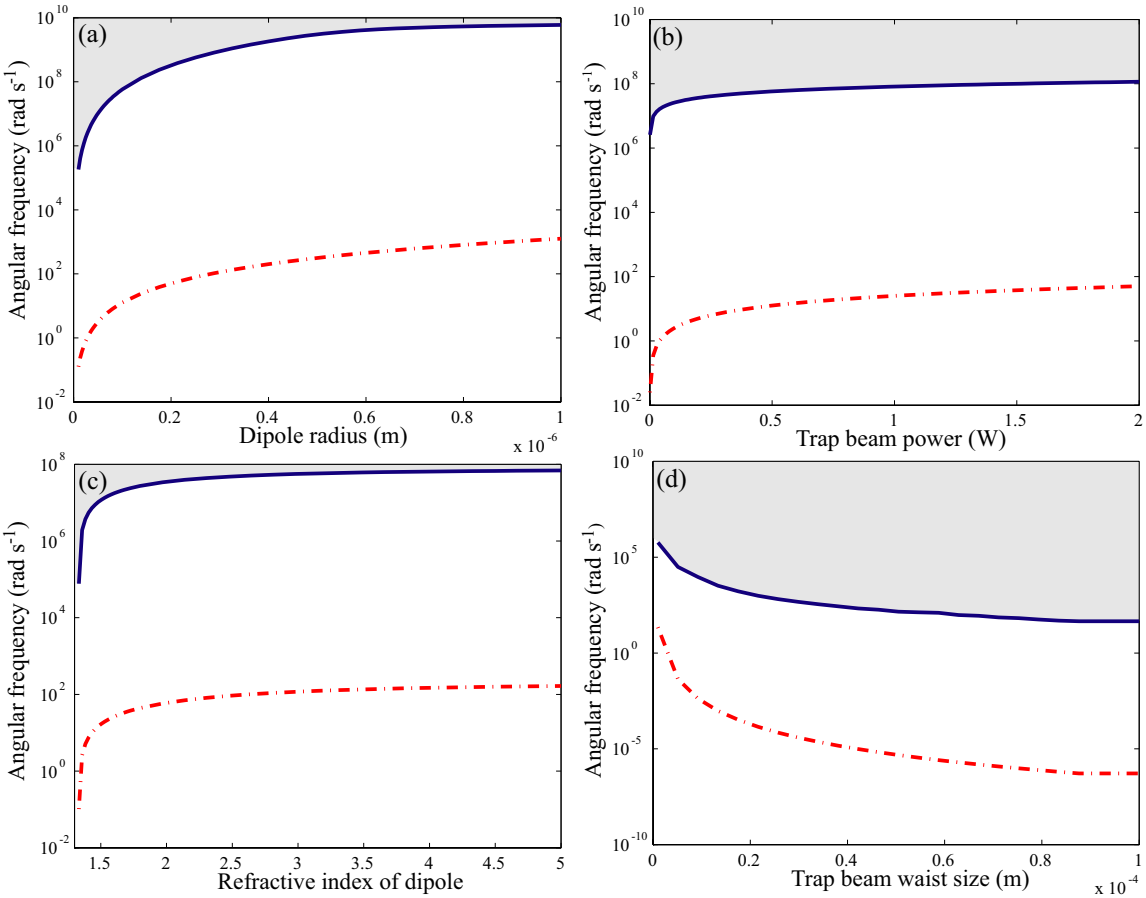

Figure 4. Crossover and corner frequencies of shotnoise and Brownian motion. The parameters varied are (a) dipole size, (b) trap beam power, (c) refractive index of the dipole and (d) waist size of the trap beam. Crossover frequencies are shown by a solid line, while critical frequencies are shown by a dot-dashed line. For frequencies above the crossover frequency, shotnoise becomes the dominant noise source, whereas at lower frequencies Brownian motion is dominant. Note that due to asymmetric effects that become important for tightly focused beams,[9] the x-axis on (d) for small waist sizes is defined to be the waist size of a paraxially approximated beam.

5. P. Galajda and P. Ormos, "Complex micromachines produced and driven by light", Appl. Phys. Lett., **78**, pp. 249, 2001; M. E. J. Friese, H. Rubinsztein-Dunlop, J. Gold, P. Hagberg, and D. Hanstorp, "Optically driven micromachines", Appl. Phys. Lett., **78**, pp. 547, 2001; M. E. J. Friese, T. A. Nieminen, N. R. Heckenberg, and H. Rubinsztein-Dunlop, "Optical alignment and spinning of laser-trapped microscopic particles", Nature, **394**, pp. 348, 1998.
6. B. Lukic, S. Jeney, C. Tischer, A. J. Kulik, L. Forr, and E.-L. Florin, "Direct observation of diffusive motion of a Brownian particle", Phys. Rev. Lett., **95**, pp. 160601, 2005; H. J. H. Clercx and P. P. J. M. Schram, "Brownian particles in shear flow and harmonic potentials: A study of long-time tails", Phys. Rev. A, **46**, pp. 1942, 1992.
7. See for example: D. Leckband, "Measuring the forces that control protein interactions", Annu. Rev. Biophys. Biomol. Struct., **29**, pp. 1, 2000.
8. A. Ashkin, J. Dziedzic, J. Bjorkholm, S. Chu, "Observation of a single-beam gradient force optical trap for dielectric particles," Opt. Lett., **11**(5), pp. 288, 1986.
9. S. Quabis, R. Dorn, M. Eberler, O. Glöckl, G. Leuchs, "The focus of light - theoretical calculation and experimental tomographic reconstruction," App. Phys. B, **72**, pp. 109, 2001.
10. B. Richards and E. Wolf, "Electromagnetic diffraction in optical systems II. Structure of the image field in an aplanatic system," P.R.L. Series A, **253**, pp. 358, 1959.

11. N. Treps, N. B. Grosse, W. P. Bowen, C. Fabre, H.-A. Bachor, and P. K. Lam. "A Quantum Laser Pointer," Science, **301**, pp. 940, 2003.
12. M. T. L. Hsu, V. Delaubert, P. K. Lam, and W. P. Bowen., "Optimal optical measurement of small displacements," J. Optics B, **6**, pp. 495, 2004.
13. Y. Harada and T. Asakura, "Radiation forces on a dielectric sphere in the Rayleigh scattering regime," Opt. Comm., **124**, pp. 529, 1996.
14. J. W. Tay and W. Bowen, in preparation.
15. T. Nieminen, H. Rubinsztein-Dunlop, N. Heckenberg, "Multipole expansion of strongly focused laser beams," JQSRT, **79-80**, pp. 1005, 2003.
16. C. Bohren and D. Huffman, *Absorption and Scattering of Light by Small Particles*, pp.139-140, Wiley-Vch, Weinheim, 2004.
17. J. Jackson, *Classical Electrodynamics: 3rd edition*, pp. 410-412, Wiley, New Jersey, 1999.
18. K. Berg-Sørensen and H. Flyvberg, "Power spectrum analysis for optical tweezers," Rev. Sci. Instrum., **75(3)**, pp. 594.
19. Z. Gong, H. Chen, S. Xu, Y. Li, and L. Lou, "Monte-Carlo simulation of optical trap stiffness measurement," Opt. Comm., **263**, pp. 229, 2006.
20. F. Gittes, C. Schmidt, "Thermal noise limitations on micromechanical experiments," Eur. Biophys. J., **27**, pp. 75, 1998.